Coherent Josephson nanostructures and the dissipation of the persistent current in the a-b planes of $YBa_2Cu_3O_{7-\delta}$ thin films

H. Darhmaoui* and J. Jung
Department of Physics, University of Alberta, Edmonton, Alberta, Canada T6G 2J1
(Received 26 June 1997)

We investigated the dissipation of the persistent current and associated vortex dynamics in $YBa_2Cu_3O_{7-\delta}$ (YBCO) thin films of high J_c, in the remanent critical magnetization regime. Ring-shaped samples were used to measure both the relaxation of the persistent current from the critical level, and the magnitude of the critical current as a function of temperature over a range of 10–90 K. The energy barrier $U_{\rm eff}(J)$ was calculated using the analysis of the relaxation data proposed by Maley *et al.* [Phys. Rev. B **42**, 2639 (1990)]. We found the correlation between the temperature dependence of the critical current $J_c(T)$ and the dependence of $U_{\rm eff}(J)$ on the current density. When $J_c(T)$ is dominated by the Ginzburg-Landau (GL)-like temperature dependence $[J_c(T) \propto (T_c - T)^{3/2}]$, the empirical formula for the energy barrier is $U_{\rm eff}(J) = a \cdot J_c(T) \cdot \exp(-(3\pi/2)J/J_{c0})$. In the Ambegaokar-Baratoff (AB) regime of $J_c(T)$, $U_{\rm eff}(J) = J_c(T)[a_1 \exp(-(3\pi/2)J/J_{c0}) + a_2 \exp(-(9\pi/2)J/J_{c0})]$. These relationships were found to describe an intrinsic property of all thin films studied, independent of the growth conditions, substrates, film thickness, T_c, and the magnitude of the critical current density J_c. The factors $-(3\pi/2)J/J_{c0}$ and $-(9\pi/2)J/J_{c0}$ in the exponents of $U_{\rm eff}(J)$ represent tilted washboard potential $U_j(\phi)/E_j = -\cos\phi - (J/J_{c0})\phi$ for an overdamped (resistively shunted) Josephson tunnel junction, locked at phases of $3\pi/2$ and $9\pi/2$. These phases correspond to the maximum resistive dissipation in a junction. The experimental data imply that the superconductor behaves like a single overdamped Josephson junction (or an extremely coherent array of resisitively-shunted Josephson junctions). The dissipation of the persistent current occurs due to the collective motion of vortices through the Josephson nanostructures in YBCO. The nanostructures have been revealed in the high-resolution electron microscope studies of Etheridge [Philos. Mag. A **73**, 643 (1996)] and in the studies of the AB to GL crossover effects in the temperature dependence of the critical current [Darhmaoui and Jung, Phys. Rev. B **53**, 14 621 (1996)]. The results favor discrete models of the physical properties of high-temperature superconductors, developed by Stroud, Emery, and Kivelson. We postulate that the vortex pinning in YBCO thin films originate from the variation of the Josephson coupling energy within the Josephson nanostructures. [S0163-1829(98)01013-3]

I. INTRODUCTION

It has been argued that the fast relaxation of the persistent current from its critical value in high-temperature superconductors can be attributed to the thermally activated motion of vortices between weak pinning centers.[1] According to the collective-pinning theory, the weak short-range disorder is responsible for the pinning.[2] Two types of pinning were considered: δT_c pinning, which is associated with disorder in the transition temperature T_c, and δl pinning, which arises from the spatial variations in the charge-carrier mean free path l near lattice defects. The critical current and the pinning energy have been studied by Griessen *et al.*[3] in $YBa_2Cu_3O_{7-\delta}$ (YBCO) thin films over a wide range of temperatures (10–80 K) using a torque magnetometer and a magnetic-field sweeping technique. The authors suggested that for $B < 2$ T and $T < 80$ K the temperature dependence of the critical current and that of the pinning energy could be understood in the framework of the δl pinning of single vortices pinned by randomly distributed weak pinning centers. Moreover, they argued that the independence of the δl-pinning mechanism on the thin-film growth conditions and substrates suggests that the source of the δl pinning is related to randomly distributed oxygen vacancies, as pointed out earlier by Tinkham.[4] Subsequent work by the same group (Ref. 5) on oxygen-deficient YBCO thin films, supported the model of a single vortex pinning by spatial fluctuations in the charge-carrier mean free path. On the other hand, it has been found (taking into account an increase in anisotropy with a decreasing oxygen content) that the pinning energy and the critical current density systematically decrease with an increasing oxygen deficiency leading to the conclusion that the oxygen vacancies are not the main source of pinning in YBCO films. Berghuis *et al.*[6] performed the current-voltage measurements in order to probe the activation barriers for flux creep in thin films of YBCO at 77 K and fields up to 8 T. They argued that in the low-field regime flux creep may be dominated by extended strong pinning centers such as densely distributed twin boundaries or screw dislocation cores. When the vortex density exceeds the density of the strong pinning centers, weakly pinned vortices start to affect the flux-creep characteristics, e.g., by shearing along strong pinning centers. Hylton and Beasley (Ref. 7) proposed a model of pinning in the CuO_2 planes of YBCO thin films with very large critical current densities. Their analysis of typical pinning energies and critical current densities indicated that the pinning is due to a very large density of point defects, beyond the density of the extended defects seen in typical transmission electron micrographs. The model predicted a spacing between defects between 38 and 53 Å which is much smaller than the typical

500 Å or higher spacing between the extended defects. The authors pointed out that if the values of 38–53 Å were the spacing between the extended defects, then the pinning energy should be about 1.3 eV, which is significantly higher than the experimental values. They suggested that the pinning must be due to a large density of local defects, caused for example by small regions of reduced-order parameter in the strongly conducting CuO_2 plane pairs.

Recent high-resolution electron microscopy investigations at 300 K by Etheridge at Cambridge University (Ref. 8) of $YBa_2Cu_3O_{7-\delta}$ ($\delta<0.1$) revealed the presence of the electron-diffraction patterns due to cells of size approximately 10–20 Å in the a-b planes, in addition to those due to twin boundaries with spacing about 500 Å. The cells form an irregular network with walls aligned about 45° to the $\langle 100\rangle$ and $\langle 010\rangle$ axes (a-b axes), and arise from a local perturbation of the charge density distribution. This is an apparently universal feature, present in YBCO samples prepared in different ways and imaged in different microscopes. It was suggested that YBCO ($\delta<0.1$) ''buckles'' into a network of slightly misaligned cells in a struggle to relieve internal stresses. The coarse order of the cells across each crystal implies the influence of long-range strain fields. The two-dimensional networks of cells are correlated along the c axis.

The presence of cells (microdomains of the order of the coherence length in size) has been also inferred independently, by us, from the temperature dependence of the critical current I_c in YBCO thin film and granular samples (Ref. 9). $I_c(T)$ was investigated over a temperature range of 10–90 K and in magnetic fields up to 700 G. The measurements were performed using superconducting rings in a persistent mode and a scanning Hall probe to record the profile of the magnetic field across the ring, generated by the persistent current at the critical level. The magnitude of I_c was deduced from the magnitude of the persistent current's self-field in the center of the ring. This technique eliminated the contribution of normal currents to the measured value of I_c and allowed one to distinguish between depairing and depinning critical currents. The results revealed the crossover between an Ambegaokar-Baratoff-like temperature dependence of the critical current at low temperatures to a Ginzburg-Landau-like $(T_c-T)^{3/2}$ dependence at high temperatures. The crossover was observed for both depairing and depinning critical currents in c-axis-oriented YBCO thin films and in a granular YBCO. The experimental data implied the presence of superconducting nanoscale domains (of an effective size of about 30–40 Å in $YBa_2Cu_3O_{7-\delta}$ of $\delta<0.1$) coupled by Josephson tunnel junctions in the a-b planes of YBCO thin films. These findings are in agreement with the Clem's model (Ref. 10) of an Ambegaokar-Baratoff (AB) to a Ginzburg-Landau (GL) crossover effects in the temperature dependence of the critical current in strongly coupled granular superconductors. According to Clem *et al.*[10] at the AB→GL crossover temperature in $I_c(T)$ of granular superconductors, the Ginzburg-Landau coherence length is of the order of the grain size. The observation of AB→GL crossover effects in YBCO, in combination with the short coherence length in this compound, indicate, therefore, the presence of a nanoscale-size granularity. The size of these nanoscale grains decreases with an increasing oxygen deficiency and with an increasing applied magnetic field. This is consistent with a decreasing AB→GL crossover temperature in the temperature dependence of the critical current measured at different magnetic fields and on samples with different transition temperatures. AB→GL crossover effects similar to those seen in YBCO thin films have been observed in the temperature dependence of the intergrain critical current of granular YBCO (with a grain size approx. 5–10 μm). These results imply that the intergrain conduction occurs through microbridges whose internal structure is identical to that of the grain, i.e., consisting of Josephson nanostructures. The experimental observations discussed above, of the presence of Josephson nanostructures in the a-b planes of $YBa_2Cu_3O_{7-\delta}$ support theoretical models developed by Stroud, Emery, and Kivelson for the analysis of various physical properties of high-temperature superconductors such as; specific heat in a magnetic field,[11] flux-flow resistivity,[12] flux pinning, and phase transitions in a superconductor with columnar defects,[13] and the effect of phase fluctuations on the low-temperature penetration depth.[14,15] A discrete representation was used in each case, in which the superconducting layers are described as an array of very small ''grains'' each comparable in size to the coherence length and coupled together by resistively shunted Josephson junctions.

The experimental and theoretical facts imply that the Josephson nanostructures in the a-b planes of YBCO should affect all the physical properties of this superconductor. According to an intriguing argument of Halbritter,[16] across CuO_2 plane interruption (caused by in-plane weak links), charge is transferred by direct and resonant tunneling in parallel, which could mimic d-wave superconductivity due to the tunnel states inside the superconducting energy gap and the spin-flip tunnel process.

One of the important questions that is related to the presence of the a-b plane Josephson nanostructures, is how this kind of structure could influence magnetic flux pinning and consequently the dissipation of the transport current. We decided to investigate this problem in c-axis-oriented YBCO thin films over a wide temperature range. We chose films of various thickness and T_c that were grown on different substrates using various deposition methods. These thin films have allowed us to study whether the dissipation is an intrinsic in nature or whether it is affected by extended defects such as twin boundaries or dislocations. We have used ring-shaped thin films in order to generate a circulating persistent supercurrent at the critical level. The persistent current's self-field was measured by a scanning Hall probe which was also applied to record the time decay of the self-field over a time scale up to 30 000 s, at temperatures over a range of 10–90 K. This procedure is equivalent to a standard procedure of measuring relaxation of remanent magnetization in a superconducting quantum interference device magnetometer. We have measured the relaxation of the persistent current from the critical level and calculated the dependence of the effective barrier $U_{\rm eff}(J)$ for vortex motion on the current density using Maley's method.[17] $U_{\rm eff}(J)$ was then compared with the temperature dependence of the critical current $J_c(T)$. An empirical formula for $U_{\rm eff}(J)$ was found to depend on a particular regime of $J_c(T)$, which is represented by either an Ambegaokar-Baratoff-like or a Ginzburg-Landau-like behavior. $U_{\rm eff}(J)$ is independent of thin-film growth conditions,

TABLE I. Superconducting transition temperature T_c at zero resistance, film thickness, critical current density J_c at 10 and 77 K, deposition method, and substrates used, are listed for all YBCO thin films that were investigated in the course of this work. Note that J_c^a denotes an ''apparent' critical current density which is defined as the ratio of the critical current I_c to the cross-sectional area A of the sample. The actual J_c may be higher if the current flow occurs through a reduced cross-sectional area A.

Sample number	T_c (K)	Film thickness (nm)	J_c^a (A/cm^2) 10 K	J_c^a (A/cm^2) 77 K	Deposition method	Substrate
1	90	500	1.1×10^7	1.5×10^6	dc-magnetron	$LaAlO_3$
2	90	130	1.8×10^7	1.2×10^6	rf-magnetron	$LaAlO_3$
3	90	200	6.4×10^6	7.1×10^5	Laser-ablation	$LaAlO_3$
4	91	200	1.8×10^7	1.7×10^6	Laser-ablation	$LaAlO_3$
5	91	200	1.8×10^7	1.7×10^6	Laser-ablation	$LaAlO_3$
6	90	100	3.3×10^7	2.3×10^6	Laser-ablation	$SrTiO_3$
7	87	280	6.5×10^6	2.4×10^5	rf-magnetron	$SrTiO_3$
8	87	120	2.3×10^7	7.1×10^5	rf-magnetron	$LaAlO_3$
9	81	350	7.9×10^6	8.2×10^4	Laser-ablation	$LaAlO_3$

substrates, film thickness and T_c, suggesting that an intrinsic property of YBCO is responsible for the dissipation of the persistent current. Discussion of these results is provided within the framework of a discrete model, in which the a-b planes are described as superconducting domains, each comparable in size to the coherence length and coupled together by resistively-shunted Josephson junctions.

II. EXPERIMENTAL PROCEDURE

A. Sample preparation

The samples used in these studies were epitaxial c-axis-oriented $YBa_2Cu_3O_{7-\delta}$ thin films grown on oriented single-crystal substrates of $LaAlO_3$ or $SrTiO_3$ heated to high temperatures between 750 and 800 °C. The films were grown using three different deposition methods: laser ablation, dc magnetron sputtering, and rf magnetron sputtering. Laser ablation is a fast deposition process which lasts approximately 5–15 min, magnetron sputter deposition, on the other hand, requires very long thin-film-growth times of the order of 10–15 h. We have investigated nine YBCO thin films which were manufactured by various laboratories. Laser-ablated films were supplied by IBM TJ Watson Research Center, McMaster University, CTF Systems, and Purdue University. The films grown using an off-axis dc magnetron sputter deposition were provided by Westinghouse STC. An off-axis rf magnetron sputter-deposition method was applied to produce YBCO thin films at University of Alberta. The thickness of the films ranged approximately from 100 up to 500 nm. We have investigated six films of $T_c=90-91$ K, two films with $T_c=87$ K, and one with $T_c=81$ K. All these films were characterized by high critical current density J_c at 10 K of $6\times10^6-3\times10^7$ A/cm^2. J_c is approximately an order of magnitude less at 77 K for all films with $T_c=90-91$ K. The basic information, such as T_c, film thickness, J_c at 10 and 77 K, deposition method and substrate, is listed in Table I for all investigated films. The films were patterned using photolithography technique in a form of rings of outer and inner diameters of 8.5 and 5.0 mm, respectively, for all samples, except sample 2 which has an outer diameter of 10 mm and an inner one of 6 mm.

B. Measurement of the persistent current relaxation and the critical current

We have measured the temperature dependence of the relaxation of the persistent current from the critical level, and the magnitude of the critical current, using ring geometry and a scanning Hall probe. The persistent current was induced in the zero-field-cooled (ZFC) ring at temperatures below T_c by applying and subsequently switching off an external magnetic field generated by a nonsuperconducting (copper-wound) solenoid. The direction of the field was parallel to the axis of the ring (the c axis of the YBCO film). The profile of the persistent current's self-field was recorded by a scanning Hall probe (of sensitive area 0.4 mm^2 and ±2 mG in sensitivity) over a scanning distance of 27 mm across the ring, and at a constant height of 2.5 mm above the ring's surface. We were able to measure both the axial (perpendicular to the rings surface) and the radial (parallel to the ring's surface) components of the self-field. The Hall probe was kept at room temperature and in air in order to avoid any offsets in the reading of the magnetic field, while the sample was in thermal contact with a copper block whose temperature was controlled over a range of 10–95 K with a GaAlAs diode and Pt resistance thermometers and an inductionless heater. An increase of the persistent current's magnitude was achieved by increasing the external magnetic field. The critical level of the persistent current was reached when the current's self-field attained a saturation. An external magnetic field less than 1 kG was sufficient to saturate the self-field over a temperature range between 10 K and T_c. The magnitude of the critical current was inferred from the saturation value of the axial component of the self-field using the Biot-Savart law. This technique allowed us to measure the temperature dependence of the critical current over a wide temperature range between 10 K and T_c (see Ref. 9 for details of the measurement procedure). Table I contains J_c at 10 and 77 K obtained with the method described above for all YBCO films used in these studies. The measurement of the persistent current's self-field also enabled us to record the relaxation (time decay) of the persistent current from various levels of the current up to the critical value. The relaxation

data were taken over a time range of 1–40 000 s at temperatures between 10 K and T_c. Figure 1(a) presents the distributions of the axial and radial components of the persistent current's self-field measured 30 and 10 000 s after the critical state was established in the zero-field-cooled ring. The profiles were scanned by a Hall probe at a distance of 3 mm above the ring. The self-field (trapped field), normalized to its value at the ring's center [Fig. 1(b)], reveals that the relaxation processes do not affect the shape of the profiles. This indicates that the normalized relaxation rate is constant across the ring and the fast decay rates are absent at the ring's outer edges. The solid lines in Fig. 1(a) represent the computer simulations of the axial field $B_z(r,z)$ and the radial field $B_r(r,z)$, using the computation methods described in Refs. 18–20. The ring was divided into 2000 concentric ring segments (of cross-sectional area $0.5\times0.5\ \mu\mathrm{m}^2$). The axial and radial fields generated by the current in each ring segment were calculated from the Biot-Savart equation.[21] The total axial and radial field above the sample was obtained by summing up the contribution from the individual current loops. Perfect fit to the experimental data was achieved with the uniform distribution of the current across the ring's width [Fig. 1(c)]. The relaxation processes affect the magnitude of the current density but not its distribution. When a critical persistent current is induced in a ring, it applies the Lorentz force on the vortices trapped in the bulk of the ring, which pushes flux lines in the radial direction out of the ring. The vortex-line motion generates the electric field $\mathbf{E}=(1/c)(\mathbf{B}^l\times\mathbf{v})$. We take $\mathbf{B}^l$ in the z direction (the ring's axis) which represents the local magnetic induction B_z^l due to the axial component of the persistent current's self-field, and $\mathbf{v}$ the drift velocity of vortices in the radial direction from the ring's axis. Then $\mathbf{E}$ is in the azimuthal direction (along the axis tangent to the ring's perimeter) and its magnitude is $E_\theta=(1/c)B_z^l v_r$. Because of the cylindrical symmetry and the independence of the vortex motion on the tangential coordinate θ, one could treat the problem as one-dimensional one and replace cylindrical coordinates (r,θ,z) with Cartesian ones (x,y,z). Then for the motion of flux in the x direction and with the local induction B_z^l, the magnitude of $\mathbf{E}$ is $E_y=(1/c)B_z^l v_x$. Using the Maxwell equation c curl $\mathbf{E}=-(\partial\mathbf{B}/\partial t)$, the equation that describes flux motion (and consequently the decay of the persistent current due to the motion of vortices in the ring's bulk) could be written in the following form:

$$\frac{\partial B_z^l}{\partial t}=-c\,\frac{\partial E_y}{\partial x}=-v_x\,\frac{\partial B_z^l}{\partial x}, \tag{1}$$

where the drift velocity v_x is taken constant along the x direction and equal to

$$v_x=\omega_0 a\,\exp[-U_{\mathrm{eff}}(J)/kT]. \tag{2}$$

Here ω_0 is the characteristic attempt frequency, a is the hopping distance, and $U_{\mathrm{eff}}(J)$ is the effective energy barrier for the thermally activated hopping. The resulting equation

$$\frac{\partial B_z^l}{\partial t}=-\omega_0 a\,\frac{\partial B_z^l}{\partial x}\exp[-U_{\mathrm{eff}}(J)/kT] \tag{3}$$

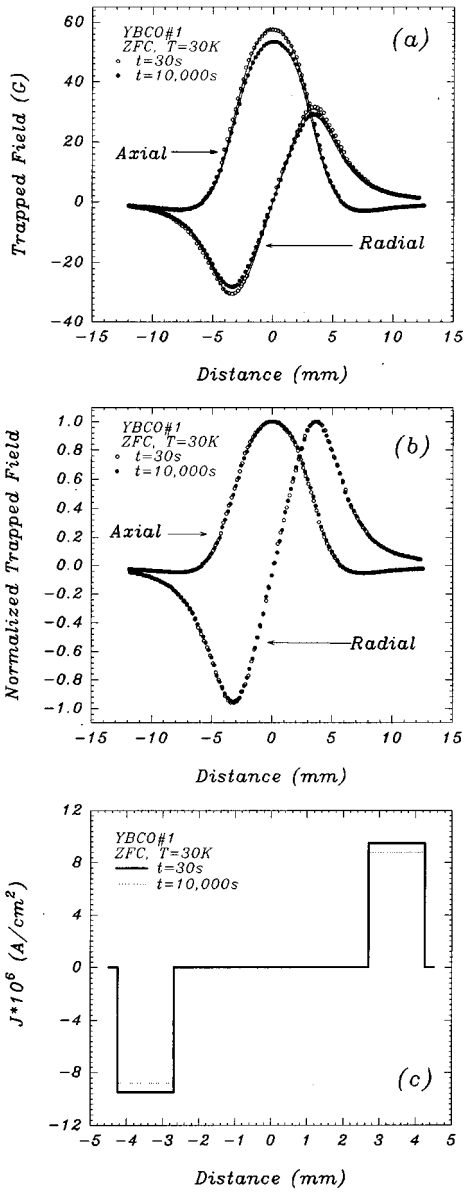

FIG. 1. (a) The profiles of the axial and radial trapped fields $B_z(r)$ and $B_r(r)$ measured across the ring of YBCO film 1 at a distance of 3 mm above it, after waiting 30 s (open circles) and 10 000 s (full circles). The profiles represent the axial and radial components of the persistent current's self-field. Distances $r=\pm2.5$ mm and $r=\pm4.25$ mm mark the inner and the outer edges of the ring. The sample was zero-field cooled down to 30 K, before an external field of 700 G was applied and subsequently reduced to zero in order to generate the persistent current at the critical level. The solid lines represent the computer simulations (see text) of the axial and radial profiles using the Biot-Savart law and the current distribution shown in (c). (b) The profiles of the axial and radial trapped field taken from (a), which are normalized using the maximum values of the axial and the radial trapped fields. Note that the shape of both profiles does not change during persistent current's decay, suggesting that the normalized decay rate remains constant across the ring. (c) The distribution of the persistent current density $J(r)$ in the zero-field cooled ring at 30 K after waiting 30 s (solid line) and 10 000 s (dotted line). This distribution was used to perform computer calculations of the profiles of the axial and radial components of the self-field of the persistent current in (a).

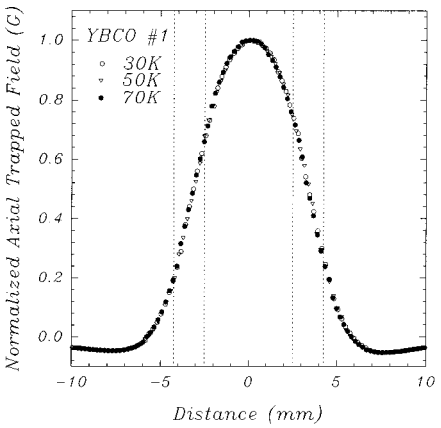

FIG. 2. The profiles of the axial component $B_z(r)$ of the persistent current's self-field at the critical value, measured at temperatures of 30 K (open circles), 50 K (open triangles), and 70 K (full circles) in the zero-field cooled ring of YBCO film 1 at a distance of 2.5 mm above it. The profiles are normalized to the value of the field at the center of the ring. Note that the shape of the profile is independent of temperature. Distances $r=\pm 2.5$ mm and $r=\pm 4.25$ mm mark the ring's inner and outer edges.

can be modified further by taking into account the gradient of B_z^l over a distance x, which was measured by a Hall probe at a height z above the ring (Fig. 2). The data show that the gradient of B_z^l is

$$\frac{\partial B_z^l}{\partial x}=-\frac{B_z^l(R_{id})-B_z^l(R_{od})}{d}\simeq-\frac{B_z^l(R_{id})}{R_{id}}, \tag{4}$$

where R_{id} and R_{od} are the inner and outer radii of the ring, respectively, and d is the width of the ring.

Equation (3) written for the local induction B_z^l at $x=R_{id}$ is

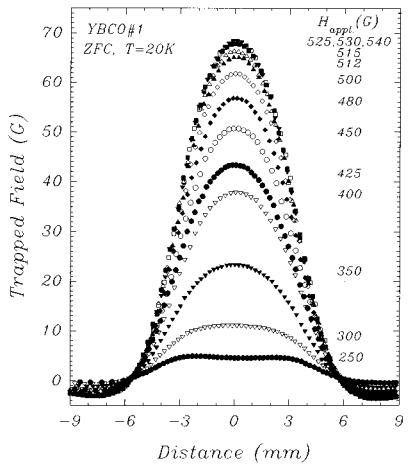

FIG. 3. The profiles of the axial component $B_z(r)$ of the self-field of the persistent currents circulating in a ring of YBCO film 1. Persistent currents, of various levels up to the critical value were induced in the ring at 20 K after an external fields between 250 and 540 G were applied to the zero-field-cooled sample. Distances $r=\pm 2.5$ mm and $r=\pm 4.25$ mm mark the ring's inner and outer edges. The profiles were measured at a distance of 2.5 mm above the ring.

$$\left.\frac{\partial B_z^l}{\partial t}\right|_{x=R_{id}}=-\omega_0 a\left.\frac{\partial B_z^l}{\partial x}\right|_{x=R_{id}}\exp[-U_{\rm eff}(J)/kT]. \tag{5}$$

Using Eq. (4), one can transform this relation to

$$\frac{\partial B_z^l(R_{id})}{\partial t}=\omega_0 a\,\frac{B_z^l(R_{id})}{R_{id}}\exp[-U_{\rm eff}(J)/kT]. \tag{6}$$

Taking into account the relationship between $B_z^l(R_{id})$ and the magnitude of the persistent current I, given by the Biot-Savart law, the decay of the persistent current is described by

$$\frac{dI}{dt}=\frac{\omega_0 a}{R_{id}}\,I\,\exp[-U_{\rm eff}(J)/kT] \tag{7}$$

or

$$\frac{dJ}{dt}=\frac{\omega_0 a}{R_{id}}\,J\,\exp[-U_{\rm eff}(J)/kT]. \tag{8}$$

The effective energy barrier can be extracted from the above equation, in the following form:

$$\begin{aligned}U_{\rm eff}(J)&=-kT\,\ln\left[\left(\frac{dJ}{dt}\right)\Big/\,J\right]+kT\,\ln\left(\frac{\omega_0 a}{R_{id}}\right)\\&=-kT\left\{\ln\left[\left(\frac{dJ}{dt}\right)\Big/\,J\right]-C\right\},\end{aligned} \tag{9}$$

where $C=\ln(\omega_0 a/R_{id})$ is a constant which is independent of the magnetic field or the current. The constant $\omega_0 a$ is a prefactor in Eq. (2) for v_x and it equals the velocity of a vortex line when the probability of each hopping process in the direction of the Lorentz force is one. Maley *et al.*[17] estimated $\omega_0 a\simeq 0.25$ m/s from the measurement of magnetic relaxation in a grain-aligned sample of YBCO powder. The upper limit of $\omega_0 a\simeq 10$ m/s for the thermally activated flux motion was estimated by Schnack *et al.*[22] They took smaller value of $\omega_0 a=2$ m/s in the calculation of the magnetic moment hysteresis loop by means of a numerical solution of the flux-creep differential equation. We used $\omega_0 a=2$ m/s and $R_{id}=2.5$ mm to obtain tentative value of $C=6.7$.

We applied Maley's method[17] in order to calculate $U_{\rm eff}(J)$ over a wide range of J. The measurement of the time decay of J from its critical value J_c at a fixed temperature, over an experimentally feasible time range of 1–100 000 s, allows the change of J by only 20%.[23] Maley *et al.* were able to extend the accessible region of J by recording the decay of magnetization from its critical value $M\propto J_c$ for various temperatures below T_c. Changing a temperature ensured a continuous change in J_c, and permitted the measurement of $U_{\rm eff}(J)$ for a wide range of current. At each temperature magnetic relaxation measurements were used to find dM/dt as a function of the current density J. As a result, a curve of $U_{\rm eff}[J(T)]$ versus $J(T)$ was produced, which consisted of multiple segments, each representing the time decay of magnetization from its critical value, measured at different temperature T. The temperature dependence in $U_{\rm eff}[J(T)]$ was eliminated by Maley *et al.* by introducing a temperature-dependent factor[24,25] $G(T)=1-(T/T_x)^2$ where T_x is a characteristic temperature taken from the magnetic irreversibility line. Plotting of $U_{\rm eff}[J(T)]/G(T)$ versus J produced a continu-

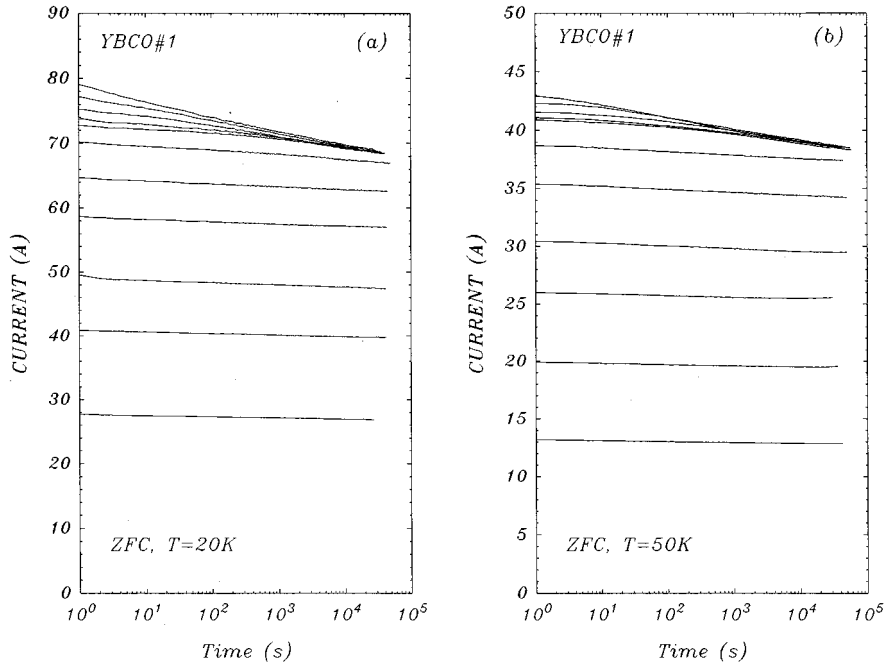

FIG. 4. The dependence of the persistent currents, of various magnitudes up to the critical value, on the logarithm of the waiting time. The decays were measured at temperatures of 20 and 50 K in the ring of YBCO film 1. The calculation of the energy barrier $U_{\text{eff}}(J)$ was based on the time decay of the persistent current from the highest value over a time interval of 2000–30 000 s. Note that the decay curves of the persistent currents close to the critical value merge after waiting approximately 1000 to 2000 s.

ous curve. However, Berghuis *et al.*[6] argued that there is an uncertainty in the Maley's temperature-dependent correction factor $G(T)$, which does not allow one to discriminate between various nonlinear scenarios for $U_{\text{eff}}(J)$.

Our procedure involves the measurements of the relaxation rates of the persistent current from the critical level as a function of the current density J for temperatures taken every 5 K between 10 and 85 K. These measurements were used to find dJ/dt vs J, whose value is necessary for the calculation of $U_{\text{eff}}(J)$ from Eq. (9).

III. EXPERIMENTAL RESULTS

The profiles of the axial component of the self-field of the persistent current circulating in zero-field-cooled rings of YBCO thin films, have been measured over a temperature range of 10–85 K. Figure 3 shows typical profiles measured at 20 K for various levels of the persistent current between zero and a critical value I_c. The decays of the persistent current have been recorded over a time range between 1 and 40 000 s, and every 5 K over a temperature range 10–85 K. Typical plots of the current versus logarithm of time for various currents between zero and I_c at 20 and 50 K are shown in Fig. 4. For currents close to I_c the initial decays up to approximately 1000 s are not fully logarithmic. After 1000 s the relaxation curves merge and a common ''steady-state'' logarithmic decay is established. The initial nonlogarithmic decay of magnetization in YBCO was reported by Gurevich and Küpfer[26] and interpreted as due to the redistribution of magnetic flux over the sample volume. Therefore, we have calculated $U_{\text{eff}}(J)$ from a steady-state logarithmic portion of the relaxation curve for waiting times between 2000 and 40 000 s. Figure 5 presents the ''Maley's'' segments of U_{eff} as a function of the current calculated from the relaxation data (which were measured every 5 between 10 K and 85 K) for six different YBCO thin films of $T_c = 90-91$ K. We have made the comparison of the dependence of U_{eff} on the cur-

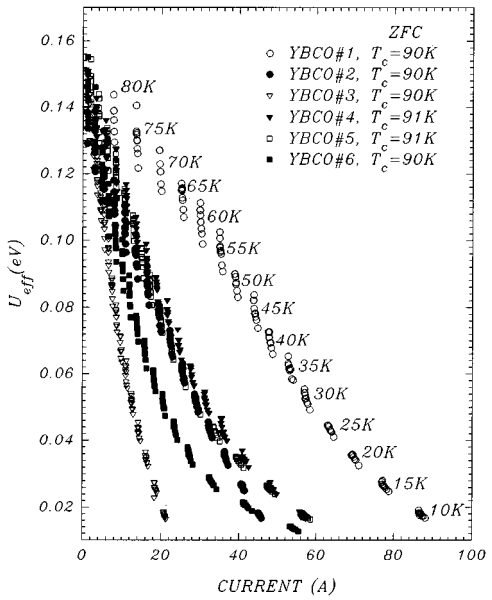

FIG. 5. The dependence of the energy barrier U_{eff} on the magnitude of the persistent current for six YBCO ring-shaped films from 1 up to 6. U_{eff} was calculated from the relaxation data (Fig. 4) using the Maley's procedure. The ''Maley's'' segments were calculated every 5 K for temperatures between 10 and 85 K.

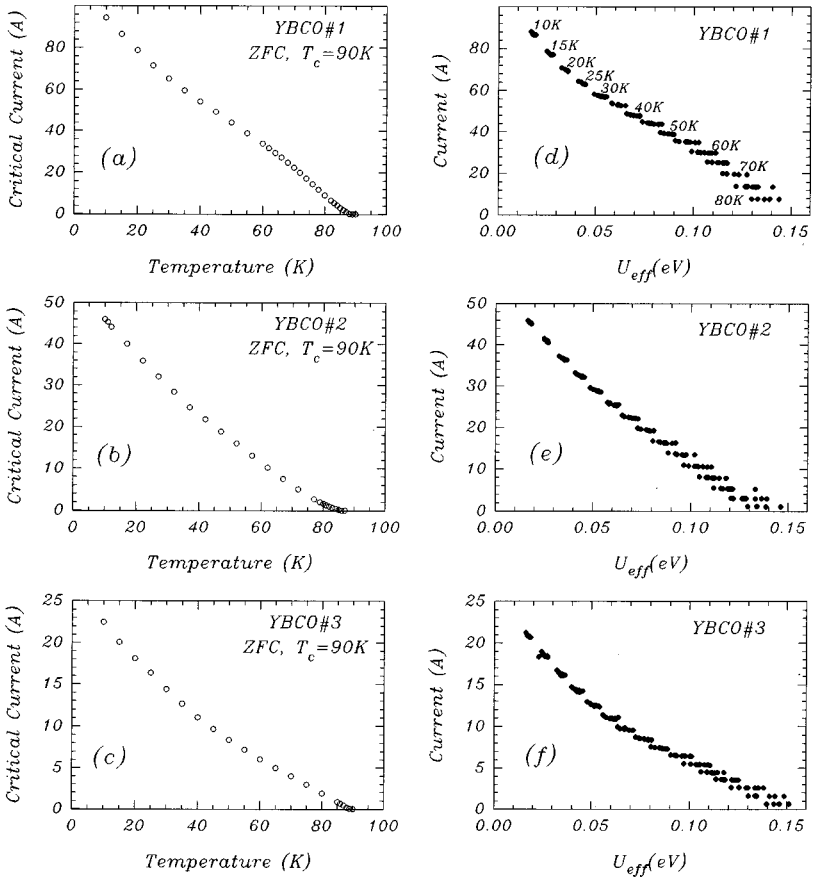

FIG. 6. The comparison of the temperature dependence of the critical current $I_c(T)$ (see figures on the left) with the dependence of the energy barrier on the current $U_{\rm eff}(I)$ (figures on the right), measured in YBCO ring-shaped films 1, 2, and 3. Note that the similarities of the shape of $I_c(T)$ to that of $U_{\rm eff}(I)$ imply that the energy barrier is a function of $I_c(T)$.

rent with the temperature dependence of the critical current (Figs. 6–8). YBCO thin films of $T_c=90-91$ K could be divided into two groups characterized by different $I_c(T)$ curves: the low-temperature reduction of I_c normalized to I_c (10 K) for YBCO films 4, 5, and 6 (Fig. 7) is larger than the corresponding decrease of I_c for YBCO films 1, 2, and 3 (Fig. 6). The temperature dependence of the critical current in YBCO films 7, 8, and 9 (Fig. 8), which have a lower T_c equal to 87 and 81 K, are essentially similar to those for YBCO with $T_c=90-91$ K. The dependence of $U_{\rm eff}$ on the current, seen in Figs. 6, 7, and 8, resembles that of the critical current on temperature. One could conclude that $U_{\rm eff}(J)$ contains the temperature dependence of J_c, which is, in fact, a consequence of the Maley's method adopted in our studies. We assume that $U_{\rm eff}(J)$ could be, therefore, written in the following form:

$$U_{\rm eff}(J)=J_c(T)\cdot F(J), \tag{10}$$

where $F(J)$ is a certain function of the current density. Equation (10) is a simplified version of a very general relation for $U_{\rm eff}(J,H,T)=G(T)[J_c(H,T)/J_c(H,0)]^P f(q,H)$, where $q=J/J_c(H,T)$ and H is the external magnetic field. This relation has been proposed by Schnack *et al.*[27] who introduced a general inversion scheme in order to obtain $U_{\rm eff}(J,H,T)$ from magnetization measurements.

The temperature dependence of J_c is not affected by the decay of the current from the critical level (Fig. 9). This means that Eq. (10) is valid over the whole experimental range of the relaxation times. In order to identify $F(J)$ we plotted $U_{\rm eff}/I_c(T)$ versus current in Fig. 10 for six YBCO films of $T_c=90-91$ K. The data imply that $F(J)$ could be represented by an exponential or a double-exponential function.

IV. DISCUSSION

The experimental data (Fig. 10) revealed that $U_{\rm eff}(J)$ is described by an exponential or a double exponential function of J, if the temperature dependence of J_c is separated from the current-dependent part of $U_{\rm eff}$ [Eq. (10)]. The question is, what is the origin of the exponential form of $U_{\rm eff}(J)$ and how it is related to the temperature dependence of the critical current density $J_c(T)$. In an attempt to answer this question, we produced two graphs for each YBCO thin film (Figs. 11, 12, and 13). The first one shows $[I_c(T)/I_c(10\ {\rm K})]^{2/3}$ versus T/T_c and the other one the logarithm of $U_{\rm eff}/I_c(T)$ versus $I/I_c(0\ {\rm K})$. Regarding the first graph, by plotting $[I_c(T)]^{2/3}$ versus temperature, we were able to separate a GL-like dependence of $I_c(T)$ from an AB-like behavior. Theoretical fits to the experimental data were performed taking a superposition of two dependences of the critical current on tempera-

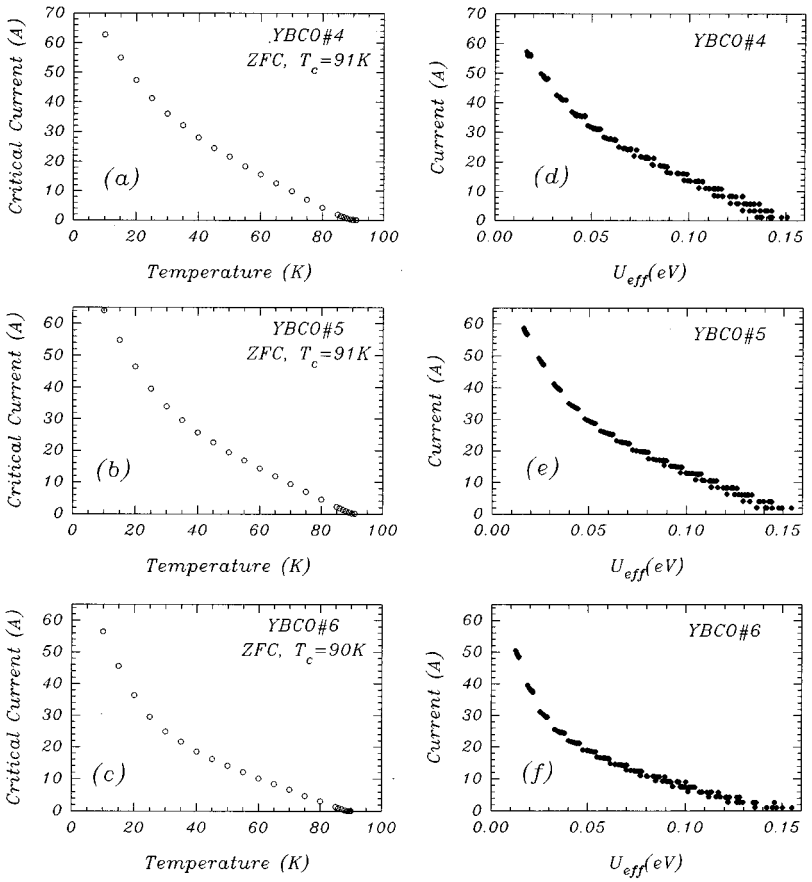

FIG. 7. The comparison of the temperature dependence of the critical current $I_c(T)$ (see figures on the left) with the dependence of the energy barrier on the current $U_{\rm eff}(I)$ (figures on the right), measured in YBCO ring-shaped films 4, 5, and 6. These films have different temperature dependence of I_c from that observed in YBCO films 1, 2, and 3 (Fig. 6), which is characterized by the larger low-temperature reduction of $I_c/I_c(10\,\mathrm{K})$. Note that the similarities of the shape of $I_c(T)$ to that of $U_{\rm eff}(I)$ imply that the calculated energy barrier is a function of $I_c(T)$.

ture: a GL-like $(T_c-T)^{3/2}$ dependence and an AB-like dependence (Fig. 14). An AB-like dependence was calculated from the Clem's model of an Ambegaokar-Baratoff to a Ginzburg-Landau crossover in $J_c(T)$ of granular superconductors (Ref. 10) using the coupling constant ε_0 as a fitting parameter. The experimental results and the theoretical fits for $I_c(T)$ in YBCO films of $T_c=87-91$ K (Figs. 11–13) suggest that high critical current density YBCO films behave like a stack of two c-axis-oriented films each having different $I_c(T)$. Earlier studies of the crossover in the temperature dependence of the critical current in YBCO [Ref. 9 and Fig. 3(a) in Ref. 28] point out that oxygen-deficient thin films are characterized by a GL-like $(T_c-T)^{3/2}$ dependence, and thin films close to the optimum doping exhibit an AB-like $I_c(T)$. Therefore, the superposition of a GL-like and an AB-like $I_c(T)$ indicates that each YBCO film may be modeled as a stack of two films of low and high oxygen deficiency.

It is important to note that the temperature dependence of the Josephson critical current calculated for optimally doped ($T_c=90$ K) YBCO with d-wave pairing[29,30] predicts the linear temperature dependence of $J_c(T)$ at low temperatures and not $(T_c-T)^{3/2}$ dependence.

At low temperatures, the AB-like part of $I_c(T)$ changes very little, and $I_c(T)$ is dominated by the GL-like dependence. Calculation of $U_{\rm eff}(J)$ according to the Maley's procedure, requires a continuous change in the critical current as a function of temperature. This means that at low temperatures, the calculated $U_{\rm eff}(J)$ should characterize flux-pinning barrier of a superconductor which exhibits a GL-like $I_c(T)$. At high temperatures close to T_c, on the other hand, $U_{\rm eff}(J)$ should describe pinning of a superconductor with an AB-like $I_c(T)$.

The comparison of the experimental data for $U_{\rm eff}/I_c(T)$ versus $I/I_c(0\,\mathrm{K})$ with those for the temperature dependence of the critical current shown in Figs. 11–13, implies that in the GL-like regime of the critical current, $U_{\rm eff}/I_c(T)$ is described by an exponential function. For the AB-like regime of $I_c(T)$, $U_{\rm eff}/I_c(T)$ is represented by a double-exponential function. Note that the straight solid lines drawn through the experimental data for $U_{\rm eff}/I_c(T)$ vs $I/I_c(0\,\mathrm{K})$ in Figs. 11–13 have similar slopes for all samples. This suggests that for thin-film superconductors with a GL-like temperature dependence of the critical current, $U_{\rm eff}/I_c(T)$ has a universal exponential form with a fixed factor in the exponent. Deviation of the data points from the solid lines for small currents (high temperatures), seen especially clearly for YBCO samples 3–6 and 8, is related to another exponential function with a fixed argument (see Fig. 15). Therefore, for thin-film superconductors with an AB-like temperature dependence of the critical current, $U_{\rm eff}/I_c(T)$ is described

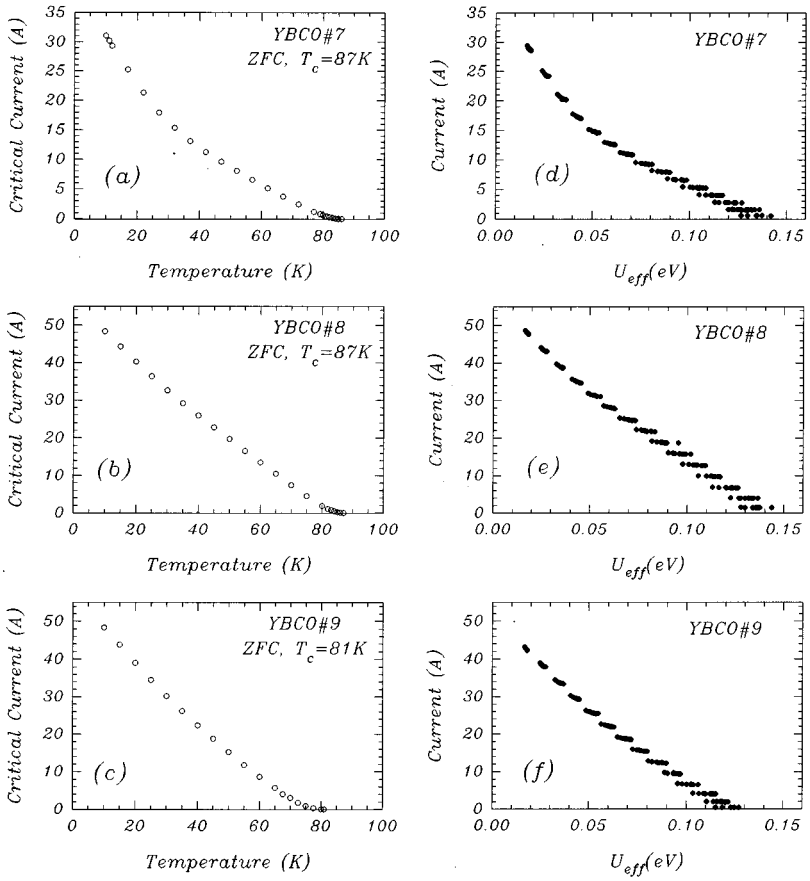

FIG. 8. The comparison of the temperature dependence of the critical current $I_c(T)$ (see figures on the left) with the dependence of the energy barrier on the current $U_{\rm eff}(I)$ (figures on the right), measured in YBCO ring-shaped films 7, 8, and 9. These films are characterized by a lower T_c than that for YBCO films from 1 to 6 (Figs. 6 and 7). Note that the similarities of the shape of $I_c(T)$ to that of $U_{\rm eff}(I)$ imply that the calculated energy barrier is a function of $I_c(T)$.

by a universal double-exponential function.

In Fig. 16, we have plotted the magnitudes of the argument of the exponents for each sample, which are represented by the slope $-\{d\ \ln[U_{\rm eff}/I_c(T)]/d[I/I_c(0\ {\rm K})]\}$. For the GL-like regime, which determines changes in $I_c(T)$ at low temperatures, this slope is $3\pi/2$. For the AB-like behavior, which dominates $I_c(T)$ at high temperatures close to T_c, $U_{\rm eff}/I_c(T)$ is a sum of two exponents with slopes of $3\pi/2$ and $9\pi/2$. The slopes for both the GL and AB-like regimes do

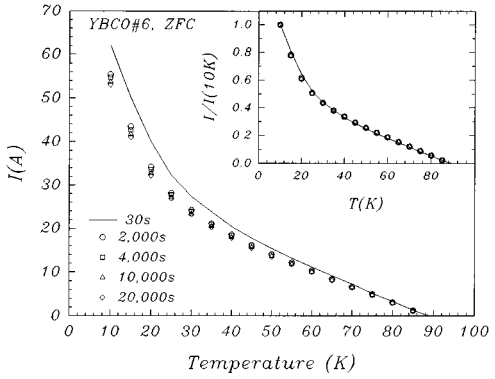

FIG. 9. The dependence of the magnitude of the persistent current I on time, measured in the ring of YBCO film 6 every 5 K over a temperature range of 10–85 K. The inset shows the same results plotted for the magnitudes of the current $I(t)$ at various times t normalized to the value of $I(t)$ at 10 K. All the data lie on the same curve, indicating that the temperature dependence of the critical current is preserved during the decay of the current.

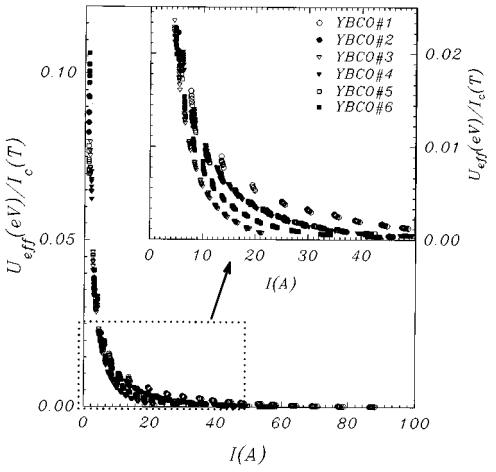

FIG. 10. The dependence of $U_{\rm eff}/I_c(T)$ on the current I presented for six YBCO thin films. The inset present the data plotted using an extended scale.

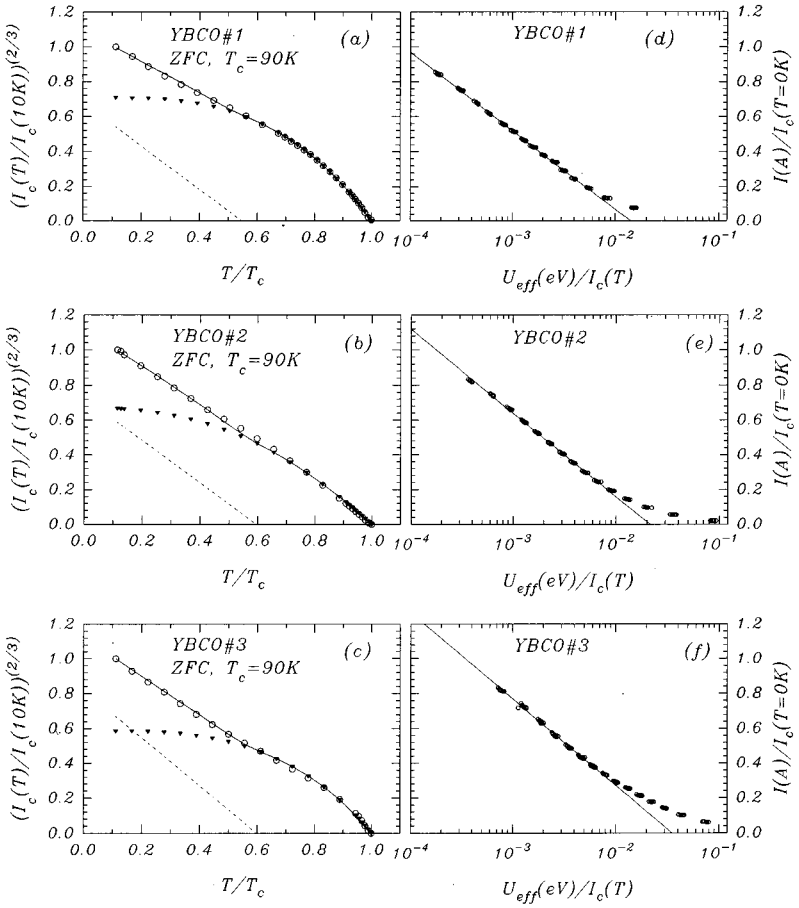

FIG. 11. The dependence of the critical current on the normalized temperature (plotted as $[I_c(T)/I_c(10\ \mathrm{K})]^{2/3}$ versus T/T_c in figures on the left) compared with the dependence of the energy barrier on the current [plotted as $U_{\mathrm{eff}}/I_c(T)$ versus I/I_c (0 K) in figures on the right] for YBCO ring-shaped films 1, 2, and 3. In (a), (b), and (c) the open circles mark the experimental data for $I_c(T)$. The solid lines represent theoretical fits to the experimental data: they are the superposition of the GL-like dependence (dashed lines) at low temperature and the AB-like dependence [Clem's model (solid triangles) with the coupling constant $\varepsilon_0=0.1$ for (a) and (c), and $\varepsilon_0=100$ for (b)]. In (d), (e), and (f) the solid straight lines indicate that the dependence of $[U_{\mathrm{eff}}/I_c(T)]$ on $I/I_c(0\ \mathrm{K})$ is exponential. Note that their slopes are sample independent.

not depend on the choice of the magnitude of the constant C in Eq. (9). However, for a constant C around 5–10, one obtains the best alignment of the Maley's segments. The experimental results provided us with the empirical formulas for $U_{\mathrm{eff}}(J)$. In the GL-like regime of $I_c(T)$

$$U_{\mathrm{eff}}(J)=aJ_c(T)\exp\left(-\frac{3\pi}{2}\frac{J}{J_{c0}}\right), \tag{11}$$

where a is a constant and J_{c0} is the critical current density at $T=0$ K. In the AB-like regime of $I_c(T)$

$$U_{\mathrm{eff}}(J)=J_c(T)\left[a_1\exp\left(-\frac{3\pi}{2}\frac{J}{J_{c0}}\right)+a_2\exp\left(-\frac{9\pi}{2}\frac{J}{J_{c0}}\right)\right], \tag{12}$$

where a_1 and a_2 are constants. Recalling the experimental observations of nanoscale-size domains coupled by Josephson tunnel junctions in the a-b planes of YBCO (Refs. 8 and 9), we identify the factors $-(3\pi/2)J/J_{c0}$ and $(9\pi/2)J/J_{c0}$ with tilted washboard potentials for overdamped (resistively-shunted) Josephson junctions which are locked at phases of $3\pi/2$ and $9\pi/2$.

According to Tinkham,[31] and Kulik and Yanson,[32] within the resistively-shunted junction model, the time dependence of the gauge-invariant phase difference ϕ in the presence of an externally supplied bias current, can be derived by equating the bias current I to the total junction current from the two parallel channels, as follows:

$$I=I_{c0}\sin\phi+V/R, \tag{13}$$

where V is a voltage difference which is maintained across the junction, R is the damping resistance, and I_{c0} is the maximum Josephson current. Eliminating V in Eq. (13), one obtains a first-order differential equation.

$$\left(\frac{\hbar}{2eRI_{c0}}\right)\frac{d\phi}{dt}+\sin\phi=\frac{I}{I_{c0}}, \tag{14}$$

where $d\phi/dt=2eV/\hbar$. Equation (14) can be written as

$$\frac{d\phi}{dt}=\frac{2eRI_{c0}}{\hbar}\left(\frac{I}{I_{c0}}-\sin\phi\right). \tag{15}$$

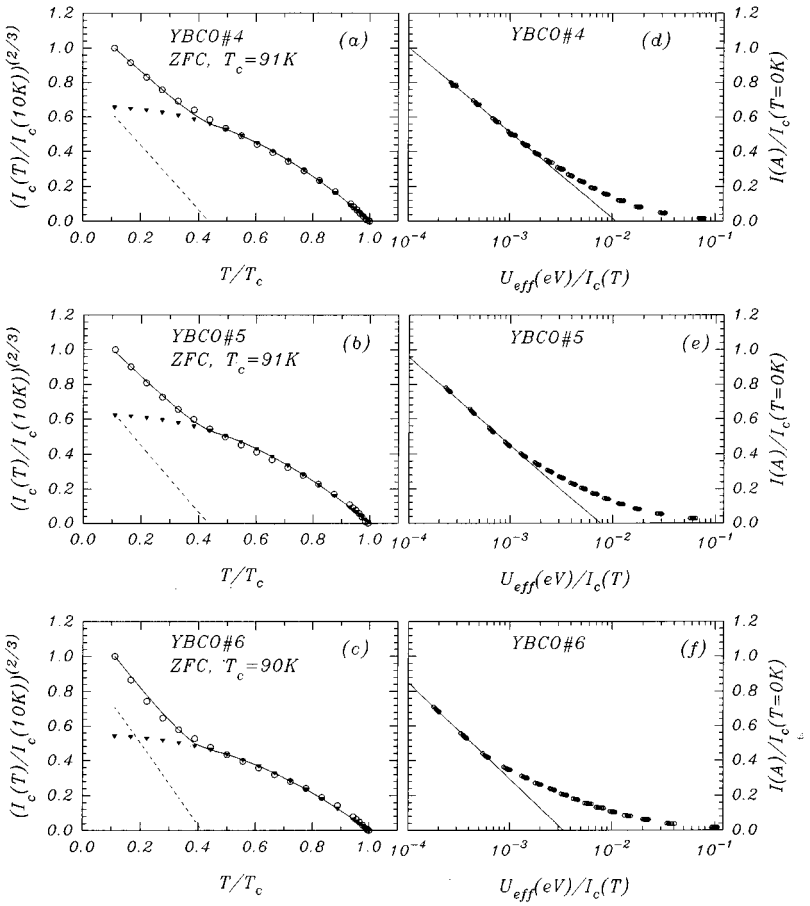

FIG. 12. The dependence of the critical current on the normalized temperature (plotted as $[I_c(T)/I_c(10\ \mathrm{K})]^{2/3}$ versus T/T_c in figures on the left) compared with the dependence of the energy barrier on the current [plotted as $U_{\mathrm{eff}}/I_c(T)$ versus $I/I_c(0\ \mathrm{K})$ in figures on the right] for YBCO ring-shaped films 4, 5, and 6. In (a), (b), and (c) the open circles mark the experimental data for $I_c(T)$. The solid lines represent theoretical fits to the experimental data: they are the superposition of the GL-like dependence (dashed lines) at low temperature and the AB-like dependence [Clem's model (solid triangles) with the coupling constant $\varepsilon_0=100$ for (a), (b), and (c)]. Note that the GL-like part of $I_c(T)$ is limited to a narrower temperature range in comparison to that for YBCO 1, 2, and 3 (Fig. 11). In (d), (e), and (f) the solid straight lines indicate that the dependence of $[U_{\mathrm{eff}}/I_c(T)]$ on $I/I_c(0\ \mathrm{K})$ is exponential. Note that their slopes are sample independent, and the same as for YBCO 1, 2, and 3 (Fig. 11).

When I only slightly exceeds I_{c0}, $d\phi/dt$ is always positive but varies periodically with $\sin\phi$. The maximum value of the instantaneous voltage is obtained when the phase passes through $3\pi/2$ mod $2\pi(\sin\phi=-1)$. This case corresponds to a maximum resistive dissipation in a Josephson junction.

Introducing the effective potential of the junction U_j as a function of ϕ

$$U_j(\phi)=-E_j\cos\phi-\left(\frac{\hbar I}{2e}\right)\phi, \tag{16}$$

where $E_j=\hbar I_{c0}/2e$ is the Josephson coupling energy, the voltage pulses correspond to the value of U_j locked at a phase of $3\pi/2$:

$$U_j\left(\frac{3\pi}{2}\right)=-\frac{3\pi}{2}\left(\frac{I}{I_{c0}}\right)E_j=-\frac{3\pi}{2}\left(\frac{J}{J_{c0}}\right)E_j. \tag{17}$$

The exponents in Eqs. (11) and (12) contain factors of $-(3\pi/2)(J/J_{c0})$ and $-(9\pi/2)(J/J_{c0})$ which represent tilted ''washboard'' potential $U_j(\phi)/E_j$ locked at phases of $3\pi/2$ and $9\pi/2$. This suggests that the effective energy barrier for vortex motion in YBCO thin films depends on the properties of intrinsic Josephson junctions. From the point of view of the vortex motion, YBCO film behaves like a single Josephson junction or a very coherent array of Josephson junctions.

Note that the current density J in Eqs. (11) and (12) represents the magnitude of the persistent current circulating in the ring. The profile of the persistent current's self-field in the ring can be simulated by that of the vortex field trapped in a disk of the diameter equal to the outer diameter of the ring. Therefore, the current density J can be also treated as that due to the total vortex current.

We interpret the dissipation of the persistent current as due to the vortex motion through the Josephson nanostructures known to be present in YBCO.[8,9] In this model the a-b planes consist of cells of a few nanometers in size (Fig. 17), which are coupled by resistively-shunted Josephson tunnel junctions. We assume that the pinning arises from a variation of the order parameter within the cell structure. The change of the order parameter from cell to cell leads to the spatial variation of the Josephson coupling energy between the cells

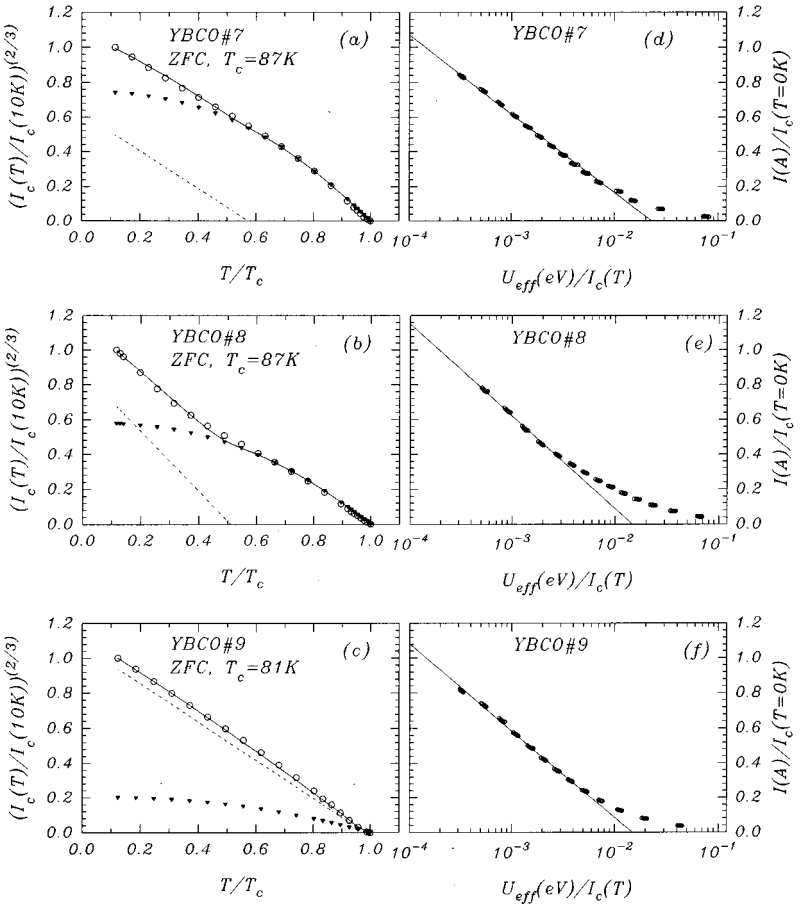

FIG. 13. The dependence of the critical current on the normalized temperature (plotted as $[I_c(T)/I_c(10\ \mathrm{K})]^{2/3}$ versus T/T_c in figures on the left) compared with the dependence of the energy barrier on the current [plotted as $U_{\mathrm{eff}}/I_c(T)$ versus $I/I_c(0\ \mathrm{K})$ in figures on the right] for YBCO ring-shaped films 7, 8, and 9, which have a lower T_c than 90 K. In (a), (b), and (c) the open circles mark the experimental data for $I_c(T)$. The solid lines represent theoretical fits to the experimental data: they are the superposition of the GL-like dependence (dashed lines) and the AB-like dependence [Clem's model (solid triangles) with the coupling constant $\varepsilon_0=100$ for (a), (b), and (c)]. In (d), (e), and (f) the solid lines indicate that the dependence of $[U_{\mathrm{eff}}/I_c(T)]$ on $I/I_c(0\ \mathrm{K})$ is exponential. Note that their slopes are sample independent and identical to those presented in Fig. 11 and 12 for YBCO 1 to 6.

in the a-b plane and between the cells on adjacent planes in the c direction. According to Clem *et al.*[10] for a square array of Josephson junctions with lattice parameter a_0, the vortex structure is determined by the array's geometry and the vortex core size is set by a_0.

We postulate that the dependence of U_{eff} on the current density J [Eqs. (11) and (12)] reflects in-phase oscillations of the Josephson array due to the collective motion of all the vortices trapped in the ring. The vortex motion occurs in the radial direction from the inner to the outer edge of the ring under the influence of the Lorentz force exerted by the circulating persistent current. The vortices travel along long Josephson junctions of the array from cell to cell. During this motion they experience a modulation of the Josephson coupling energy on a scale of a few nanometers. A possible scenario for the dissipation of energy in the array involves vortex currents which sweep the array and act as bias currents for Josephson junctions between the array's cells. Because of the modulation of the Josephson coupling energy in the array, if the sum of the vortex current and the persistent current exceeds the Josephson critical current for junctions of the weakest coupling, the phase-dependent voltage appears in the array. Maximum resistive dissipation is expected for the case of a spatial phase coherence.

Calculation of the power spectrum of the voltage in a $\mathrm{Nb/AlO_x/Nb}$ square array of Josephson junctions for different levels of the bias current has been performed recently by Lachenmann *et al.*[33] For large bias currents above the array's critical current, junctions in the array oscillate coherently and the power spectrum $S(\nu)$ consists of sharp peaks at equal multiples of frequency $\nu=eVR_s i_c/\pi\hbar$ (where R_s is the shunt resistance and i_c is the critical current of each junction in the array).

These results imply that the phase coherence at $3\pi/2$ and $9\pi/2$ observed in our experiments could represent the first and the third harmonics of coherent oscillations of the Josephson-junction array.

According to our interpretation, dissipation of the persistent current could be caused by the motion of Josephson vortices in the array. Due to a curvature of magnetic flux lines trapped in the c-axis-oriented ring, the vortex lines form an angle with the direction perpendicular to a-b planes (c-axis direction). In a layered superconductor, these vortices are viewed as chains of two-dimensional pancake vortices

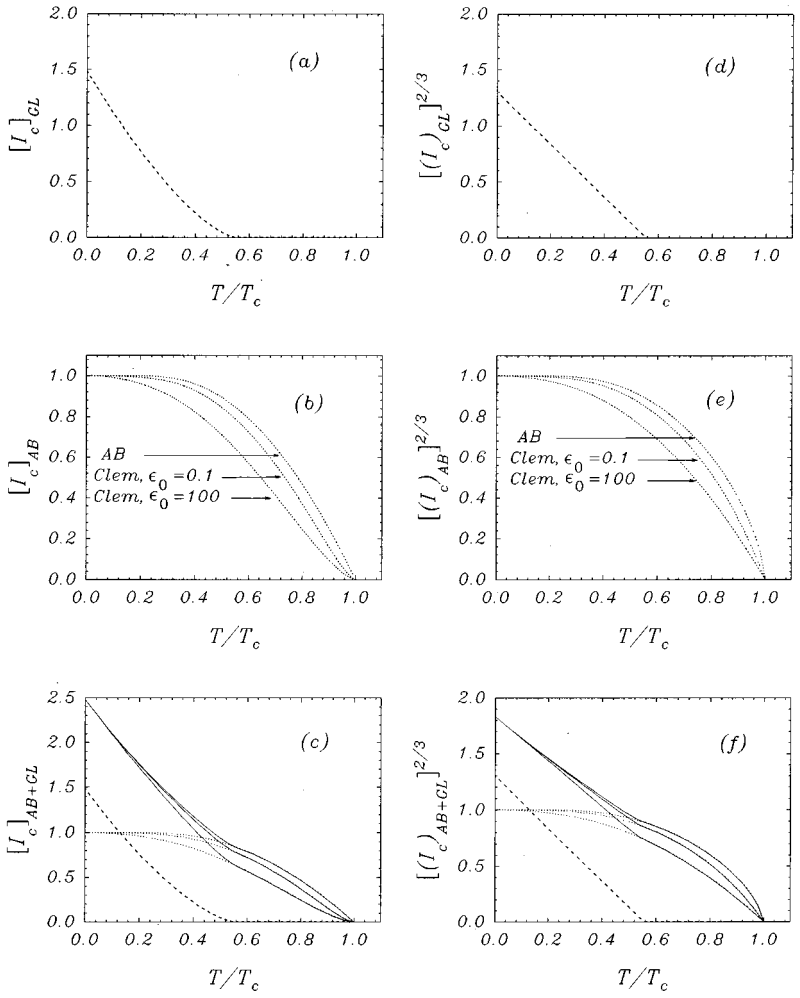

FIG. 14. The dependence of the critical current I_c on the normalized temperature T/T_c, according to various theoretical models which were utilized in the fits to the experimental data shown in Figs. 11, 12, and 13 (a), (b), and (c). (a) and (b) show a GL-like $(T_c-T)^{3/2}$ dependence of $I_c(T)$, AB dependence of $I_c(T)$, and Clem's calculations of the crossover from AB to GL in $I_c(T)$ with coupling constants $\varepsilon_0=0.1$ and 100. (c) presents a superposition of the GL-like $I_c(T)$ with that of Ambegaokar-Baratoff and Clem. (d), (e), and (f) contain the results of (a), (b), and (c), plotted as $[I_c(T)]^{2/3}$ versus T/T_c.

connected by interplane Josephson-type vortices.[34] A pancake vortex can be viewed as a finite segment of height equal to the interlayer spacing, of an Abrikosov vortex directed along the c axis.

The data obtained from our relaxation measurements show that there is a relationship between the temperature dependence of the critical current $I_c(T)$ and the relaxation of the persistent current. We assume that when the temperature dependence of I_c is GL-like, the supercurrent does not ''see'' the Josephson nanostructures in the a-b planes. Therefore, the vortex segments perpendicular to the planes are Abrikosov-like. The interplane segments which join the Abrikosov ones are the Josephson strings which experience the spatial modulation of the Josephson coupling energy between the planes. Persistent current circulating in the ring exerts the Lorentz force on the Abrikosov segments but not on the Josephson strings. The Josephson strings move between the planes due to the drag force applied to them by the Abrikosov segments. In this case the energy barrier for vortex motion $U_{\rm eff}(J)$, [expressed by Eq. (11)] should be determined solely by the spatial variation of the Josephson coupling energy between the planes. When the temperature dependence of I_c is AB-like, the supercurrent flows through the Josephson nanostructures in the a-b planes. Therefore, the in-plane pancake vortices change their character from Abrikosov- to Josephson-like. The flux lines experience the modulation of the Josephson coupling energy both in the a-b planes and between the planes. In this case, the first exponent with a phase of $3\pi/2$ in the expression for $U_{\rm eff}(J)$ [Eq. (12)] is determined by the spatial variation of the Josephson coupling energy between the planes, similarly to the GL-like case described above. The second exponent with a phase of $9\pi/2$ is attributed to the modulation of the Josephson coupling within the array in the a-b planes.

Additional experimental evidence which relates the exponent with a phase of $3\pi/2$ to the motion of the interplane Josephson vortices in a superconductor with a GL-like $I_c(T)$ in the a-b planes, has been provided by the measurements on YBCO thin film 9 with $T_c=81$ K [Figs. 13(c) and 13(f)]. The temperature dependence of the critical current in this sample is dominated by the GL-like regime [Fig. 13(c)] over a wide temperature range of 10–60 K. The reduction of the

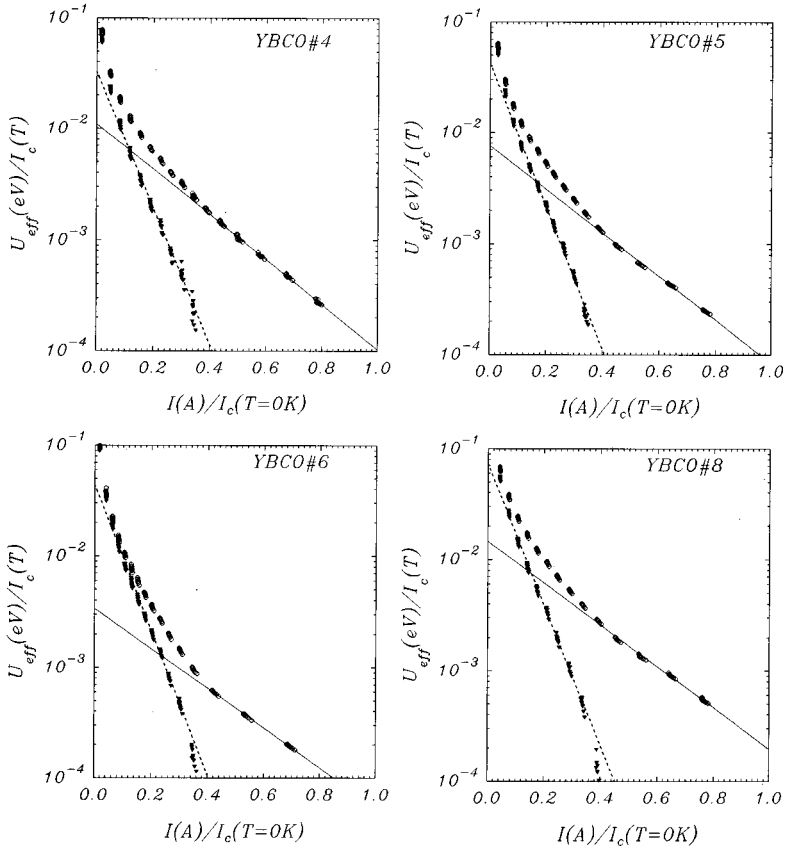

FIG. 15. The dependence of the energy barrier $[U_{\rm eff}/I_c(T)]$ on the normalized current $I/I_c(0\,{\rm K})$ plotted for YBCO ring-shaped films 4, 5, 6, and 8. These films are characterized by the pronounced AB-like behavior of $I_c(T)$ close to T_c (Figs. 11, 12, and 13), and the deviation of $[U_{\rm eff}/I_c(T)]$ from the straight solid line at small currents. The segments on the dashed lines represent the data obtained by subtracting $[U_{\rm eff}/I_c(T)]$ at low currents from the solid lines. In these cases $[U_{\rm eff}/I_c(T)]$ is a double-exponential function of $I/I_c(0\,{\rm K})$.

AB-like contribution to $I_c(T)$ at low temperatures by a factor of 3–4 in comparison to that in other samples, does not change the magnitude of the phase in Eq. (11).

Recent measurements of the microwave surface impedance in the a-b planes of ultrapure YBCO single crystals[35] performed by Zhai *et al.*[36] imply that the crystal responds like a single Josephson junction (or a coherent array of Josephson junctions) to an ac-drive current in the a-b plane. Their data were analyzed using a resistively-shunted Josephson junction model. The authors concluded that the extraordinary coherence of the data suggests an intrinsic effect, however, they expressed doubts that defects like twin boundaries in YBCO crystals could respond in such a coherent manner.

We have ruled out that the structure of the twin boundaries in YBCO thin films is responsible for the observed vortex motion and consequently for the dissipation of the persistent current. This is the result of the independence of the experimental data for the energy barrier $U_{\rm eff}(J)$ and the critical current $I_c(T)$, on the growth conditions of YBCO thin films, substrates, film thickness and the magnitude of the critical current density J_c. The structure of the twin boundaries is known to be sensitive to oxygen content.[37,38] Since $U_{\rm eff}(J)$ is also independent of T_c [see Fig. 13(d), 13(e), and 13(f)], this is an additional evidence that the energy barrier for vortex motion is not affected by the presence of extended defects in the films. Similar conclusions about the role of extended defects in the pinning mechanism in YBCO have been also drawn by Griessen *et al.*[3] in his work on pinning in YBCO thin films.

According to earlier results (e.g., Ref. 9) and Halbritter's model,[39] the major channel of the supercurrent conduction across the grain boundaries is established through the intergrain strong links. These strong links are the microbridges whose structure is the same as the grain, i.e., consists of Josephson nanostructures. The twin boundary layer thickness was found to be between 10 and 20 Å in optimally doped YBCO.[37] This is of the order of the cell size in the Josephson array in the a-b planes of YBCO. This means that the temperature dependence of the critical current in this case is governed by the Josephson tunnel junctions in the array and the weakly pinned vortices are able to shear along these which are strongly pinned by the grain boundaries such as twin boundaries or high angle boundaries.

The empirical formulas for the energy barrier given by Eqs. (11) and (12) should be modified in order to include the condition $U_{\rm eff}(J_c)=0$. We could write $U_{\rm eff}(J)$ in the form $U_{\rm eff}(J)=J_c(T)\cdot F(J)$, like in Eq. (10) where $F(J)=a\,\exp(-(3\pi/2)J/J_{c0})$ for a GL-like regime of $I_c(T)$, and $F(J)=a_1\,\exp(-(3\pi/2)J/J_{c0})+a_2\,\exp(-(9\pi/2)J/J_{c0})$ for an AB-like behavior of $I_c(T)$. The new version of the energy barrier should be represented by

$$U_{\rm eff}=J_c(T)[F(J)-F(J_c)] \tag{18}$$

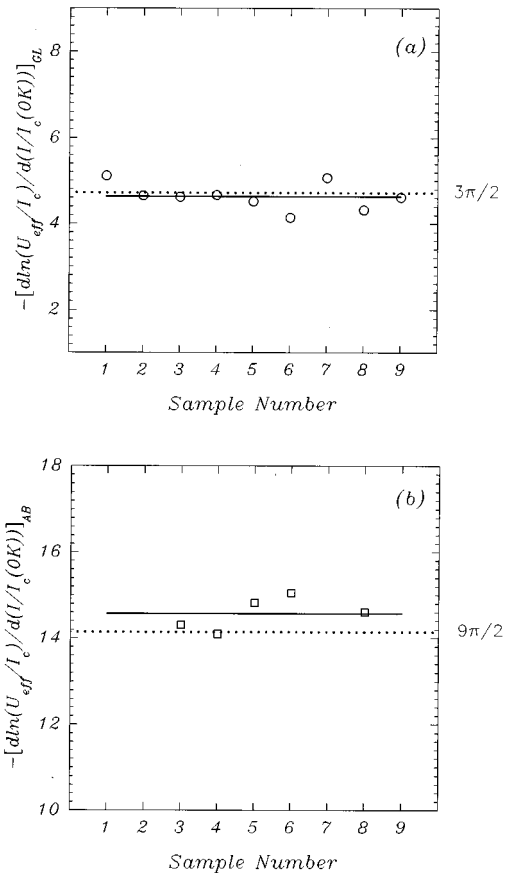

FIG. 16. The magnitudes of the argument in the exponents of $[U_{\rm eff}/I_c(T)]$ for each YBCO thin-film sample, which are represented: (a) by the slope of the straight solid lines in Figs. 11, 12, and 13 (d), (e), and (f) for the GL-like regime of $I_c(T)$; and (b) by the slope of the straight dashed lines in Fig. 15 for the AB-like regime of $I_c(T)$.

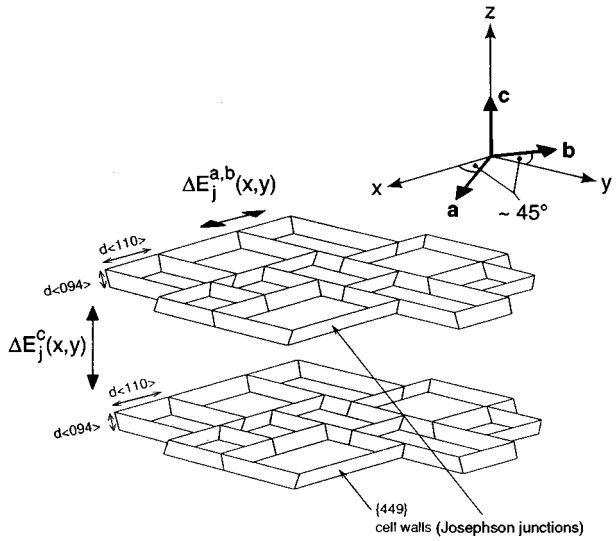

FIG. 17. The schematic of the nanoscale cells (a few nm in size) in the a-b planes of YBCO as described by Etheridge (Ref. 8) on the basis of the high-resolution electron microscopy. According to our studies, the walls between the cells form Josephson tunnel junctions with the spatial variation of the coupling energy in the a-b planes $\Delta E_j^{a,b}(x,y)$ and between the planes $\Delta E_j^{c}(x,y)$. Crystallographic directions of the cell walls are along the x,y axes. The a,b axes are positioned at an angle of about 45° relative to the x,y axes.

for both cases.

A very good fit of the experimental results for $U_{\rm eff}(J)$ in a TIBCCO (2223) single crystal to a double-exponential function has been produced by Mexner *et al.*[40] The authors applied Maley's method to calculate $U_{\rm eff}(J)$ from the relaxation data taken at magnetic fields up to 12 T and over a temperature range of 4–77 K. The analysis of the data was, however, based on the collective flux-creep model of Feigelman *et al.*[1] with the power-law dependence of the energy barrier on J.

V. SUMMARY AND CONCLUSIONS

We have measured the relaxation of the persistent current from the critical level in the a-b planes of ring-shaped YBCO thin films over a temperature range 10–90 K. We applied Maley's method[17] to calculate the dependence of the energy barrier for vortex motion on the current density $U_{\rm eff}(J)$. We found the correlation between the temperature dependence of the critical current $I_c(T)$ and the empirical form of $U_{\rm eff}(J)$. The empirical formulas for $U_{\rm eff}(J)$ are exponential. The exponential factors represent the tilted washboard potentials for an overdamped Josephson junction, locked at phases of $3\pi/2$ and $9\pi/2$. For a GL-like ($T_c - T)^{3/2}$ regime of $I_c(T)$ at low temperatures, $U_{\rm eff}(J)$ is governed by the Josephson potential with a phase of $3\pi/2$. For an AB-like behavior of $I_c(T)$, $U_{\rm eff}(J)$ is described by a double-exponential function with the Josephson potentials locked at phases of $3\pi/2$ and $9\pi/2$. From the point of view of vortex motion, YBCO thin films behave like a single resistively-shunted Josephson junction or an extremely coherent array of resistively-shunted Josephson junctions. This behavior is independent of the growth conditions of the YBCO films, film thickness, substrates, and the magnitude of J_c and T_c. We interpret the dissipation of the persistent current as due to the collective motion of vortices through the nanoscale array of overdamped Josephson junctions. The array is associated with the presence of superconducting cells, each of the size of the order of the coherence length, in the a-b planes of YBCO.[8,9] These cells are coupled by Josephson tunnel junctions in the a-b planes and between the adjacent planes in the c direction. The pinning of vortices arises from the modulation of the Josephson coupling energy in these junctions. The motion of Josephson vortices is responsible for spatially coherent voltage oscillations in the array, with phases of $3\pi/2$ and $9\pi/2$ which could represent the first and the third harmonics.

The coherent oscillations of the Josephson-junction array suggest an intrinsic mechanism of dissipation. The experimental results imply that the dissipation of the persistent current due to the motion of vortices through Josephson nanostructures, is a universal phenomenon, which describes behavior of the relaxation of magnetization in YBCO thin films.

Our investigations have generated the following open questions about the origin of both the exponential form of

the energy barrier [Eqs. (11) and (12)] and the Josephson nanostructures in the a-b planes of YBCO:

(1) Does the exponential form of the energy barrier, with the phase locking and the missing factor of kT in the exponents, imply quantum resonant tunneling of vortices through a coherent array of Josephson junctions?
(2) Is the phase separation (stripe phases) responsible for the formation of the nanoscale cell structure in the a-b planes of YBCO and consequently for the Josephson nanostructures?

Regarding the exponential energy barrier, it is similar in form to the effective Euclidean action $S_E^{(\mathrm{eff})}$, which determines the tunneling rate of vortices through a barrier during quantum tunneling process.[41] If the pinning in the Josephson nanostructures is determined by the variation of the Josephson coupling energy over distances comparable to the cell size, one could expect very narrow barriers with a large curvature of the potential at the top of the barrier. This would rise the barrier frequency and decrease the tunneling time, leading to an increase of the crossover temperature from the quantum to the classical regime.[42] Another question is how the spatial coherence of the Josephson-junction array could enhance the quantum resonant tunneling of Josephson vortices.

Regarding the origin of the nanoscale cell structure in the a-b planes of YBCO, Etheridge[8] has suggested that the cells are formed in struggle to relieve intralayer internal stresses. However, it may be important to investigate a relationship between these cells and the stripe phases which intersect, forming the superconducting islands separated by antiferromagnetic regions (see Ref. 43 for the extensive review of stripe phases in cuprates). Such a relationship would mean that the Josephson nanostructures are formed by antiferromagnetic insulating layers which couple superconducting cells.

ACKNOWLEDGMENTS

We are grateful to J.S. Preston and R. Hughes of McMaster University; A.A. Fife of CTF Systems; J.Z. Sun of IBM T.J. Watson Research Centre; J. Talvacchio of Westinghouse STC and M.W. McElfresh of Purdue University for supplying us with YBCO thin films. We are pleased to acknowledge useful discussions with E. Simánek, J.R. Clem, D.J. Scalapino, S. M. Girvin, S. Sridhar, M.R. Beasley, R.C. Dynes, R.S. Markiewicz, S.A. Kivelson, and J.D. Halbritter. This work was supported by a grant from the Natural Sciences and Engineering Council of Canada (NSERC).

*Present address: School of Science and Engineering, Alakhawayn University, Ifrane 53000, Morocco.

[1] M. V. Feigelman, V. B. Geshkenbein, A. I. Larkin, and V. M. Vinokur, Phys. Rev. Lett. **63**, 2303 (1989).
[2] G. Blatter, M. V. Feigelman, V. B. Geshkenbein, A. I. Larkin, and V. M. Vinokur, Rev. Mod. Phys. **66**, 1125 (1994).
[3] R. Griessen, Wen Hai-hu, A. J. J. van Dalen, B. Dam, Y. Rector, and H. G. Schnack, Phys. Rev. Lett. **72**, 1910 (1994).
[4] M. Tinkham, Helv. Phys. Acta **61**, 443 (1988).
[5] A. J. J. van Dalen, R. Griessen, S. Libbrecht, Y. Bruynseraede, and E. Osquiguil, Phys. Rev. B **54**, 1366 (1996).
[6] P. Berghuis, R. Herzog, R. E. Somekh, J. E. Evetts, R. A. Doyle, F. Baudenbacher, and A. M. Campbell, Physica C **256**, 13 (1996).
[7] T. L. Hylton and M. R. Beasley, Phys. Rev. B **41**, 11 669 (1990).
[8] J. Etheridge, Philos. Mag. A **73**, 643 (1996).
[9] H. Darhmaoui and J. Jung, Phys. Rev. B **53**, 14 621 (1996).
[10] J. R. Clem, B. Bumble, S. I. Raider, W. J. Gallagher, and Y. C. Shih, Phys. Rev. B **35**, 6637 (1987).
[11] C. Ebner and D. Stroud, Phys. Rev. B **39**, 789 (1989).
[12] K. H. Lee and D. Stroud, Phys. Rev. B **46**, 5699 (1992).
[13] K. H. Lee, D. Stroud, and S. M. Girvin, Phys. Rev. B **48**, 1233 (1993).
[14] E. Roddick and D. Stroud, Phys. Rev. Lett. **74**, 1430 (1995).
[15] V. J. Emery and S. A. Kivelson, Phys. Rev. Lett. **74**, 3253 (1995).
[16] J. Halbritter, J. Low Temp. Phys. **105**, 1249 (1996).
[17] M. P. Maley, J. O. Willis, H. Lessure, and M. E. McHenry, Phys. Rev. B **42**, 2639 (1990).
[18] M. Däumling and D. C. Larbalestier, Phys. Rev. B **40**, 9350 (1989).
[19] L. W. Conner and A. P. Malozemoff, Phys. Rev. B **43**, 402 (1991).
[20] D. J. Frankel, J. Appl. Phys. **50**, 5402 (1979).
[21] W. R. Smythe, *Static and Dynamic Electricity* (McGraw-Hill, New York, 1950), p. 271.
[22] H. G. Schnack, R. Griessen, J. G. Lensink, C. J. van der Beek, and P. H. Kes, Physica C **197**, 337 (1992).
[23] I. Isaac, J. Jung, M. Murakami, S. Tanaka, M. A-K. Mohamed, and L. Friedrich, Phys. Rev. B **51**, 11 806 (1995).
[24] P. J. Kung, M. P. Maley, M. E. McHenry, J. O. Willis, J. Y. Coulter, M. Murakami, and S. Tanaka, Phys. Rev. B **46**, 6427 (1992).
[25] P. J. Kung, M. P. Maley, M. E. McHenry, J. O. Willis, M. Murakami, and S. Tanaka, Phys. Rev. B **48**, 13 922 (1993).
[26] A. Gurevich and H. Küpfer, Phys. Rev. B **48**, 6477 (1993).
[27] H. G. Schnack, R. Griessen, J. G. Lensink, and H. H. Wen, Phys. Rev. B **48**, 13 178 (1993).
[28] E. C. Jones, D. K. Christen, J. R. Thompson, R. Feenstra, S. Zhu, D. H. Lowndes, J. M. Phillips, M. P. Siegal, and J. D. Budai, Phys. Rev. B **47**, 8986 (1993).
[29] R. J. Radtke, C. N. Lau, and K. Levin, J. Supercond. **8**, 499 (1995).
[30] R. J. Radtke and K. Levin, Physica C **250**, 282 (1995).
[31] M. Tinkham, *Introduction to Superconductivity* 2nd ed. (McGraw-Hill, New York, 1996), pp. 205–206.
[32] I. O. Kulik and I. K. Yanson, *The Josephson Effect in Superconductive Tunnelling Structures* (Israel Program for Scientific Translations, Jerusalem, 1972).
[33] S. G. Lachenmann, T. Doderer, R. P. Huebener, T. J. Hagenaars, J. E. van Himbergen, P. H. E. Tiesinga, and J. V. Jose, Phys. Rev. B **56**, 5564 (1997).
[34] J. R. Clem and M. W. Coffey, Phys. Rev. B **42**, 6209 (1990).
[35] A. Erb, E. Walker, and R. Flukiger, Physica C **258**, 9 (1996).
[36] Z. Zhai, H. Srikanth, S. Sridhar, A. Erb, E. Walker, and R. Flukiger, Physica C **282-287**, 1601 (1997).
[37] Y. Zhu, M. Suenaga, Y. Xu, R. L. Sabatini, and A. R. Mooden-

baugh, Appl. Phys. Lett. **54**, 374 (1989).
[38] Y. Zhu, M. Suenaga, J. Tafto, and D. O. Welch, Phys. Rev. B **44**, 2871 (1991).
[39] J. Halbritter, Phys. Rev. B **46**, 14 861 (1992).
[40] W. Mexner, J. Hoffmann, S. Heede, K. Heinemann, H. C. Freyhardt, F. Ladenberger, and E. Schwarzmann, Z. Phys. B **101**, 181 (1996).
[41] G. Blatter and V. Geshkenbein, Phys. Rev. B **47**, 2725 (1993).
[42] E. Šimánek (private communication).
[43] R. S. Markiewicz, J. Phys. Chem. Solids **58**, 1179 (1997).